Int. J. Electrochem. Sci., 13 **(2018)** 7111 – 7120, doi: 10.20964/2018.07.75

International Journal of ELECTROCHEMICAL SCIENCE
www.electrochemsci.org

Three-dimensional Ni_3Sn_4 Negative Electrodes for Lithium-Ion Batteries

Arailym Nurpeissova[1,2,*], *Akylbek Adi*[1,2], *Assylzat Aishova*[1,2], *Aliya Mukanova*[1,3], *Sung-Soo Kim*[4], *Zhumabay Bakenov*[1,2,3]

[1] National Laboratory Astana, 53 Kabanbay Batyr Ave., Astana 010000, Kazakhstan
[2] Institute of Batteries, Block 13, 53 Kabanbay Batyr Ave., Astana 010000, Kazakhstan
[3] School of Engineering, Nazarbayev University, 53 Kabanbay Batyr Ave., Astana 010000, Kazakhstan
[4] Graduate School of Energy Science and Technology, Chungnam National University, 99 Daehak ave., Yuseong-gu, Daejeon 34134, Republic of Korea
[*]E-mail: arailym.nurpeissova@nu.edu.kz

Received: 9 March 2018 / *Accepted:* 10 May 2018 / *Published:* 5 June 2018

Three-dimensional alloy based Ni_3Sn_4 negative electrodes were fabricated by simple electrodeposition technique on a mesoporous nickel foam substrate to improve the capacity and cyclability of Ni_3Sn_4 anodes for lithium-ion batteries. The combination of thin film geometry with three-dimensional foam structure is aimed to optimize the ionic/electronic current paths, and to accommodate the mechanical stresses induced by the volume changes in the electrode during repeated cycling. The surface morphology of the obtained Ni_3Sn_4 alloy electrodes was characterized by scanning electron microscopy coupled with energy-dispersive X-ray spectroscopy. X-ray diffraction analysis was performed to characterize the phases and possible impurities present in the alloy. The electrochemical features of the electrodes were investigated by cyclic voltammetry and galvanostatic charge-discharge test experiments. Obtained results showed that the as-prepared three-dimensional Ni_3Sn_4 anodes are capable of providing satisfactory lithium storage and promising cycling performance.

Keywords: Three-dimensional anode; electrodeposition; Ni_3Sn_4 alloy; lithium-ion battery

1. INTRODUCTION

The development of new electronic devices and their miniaturization is one of the major tendencies of the recent decade. Due to the application of such devices in various fields of industry, they play a critical role in potential advancements in these areas. Their reliability and, especially, ability to provide prolonged operation, are the most crucial among other important properties required

for such applications. In order to satisfy these strict requirements for implementation, next-generation power sources such as advanced rechargeable batteries are needed to satisfy prolonged operation/run on one charge. Nonetheless, it is becoming difficult for even ubiquitous lithium-ion batteries (LIBs) to meet the elevated power consumption demand in advanced devices. Therefore, new approaches should be considered to improve the performance of batteries via searching for new storage materials, improvement of existing promising materials or considering the innovative concept, design, and architecture.

Traditional LIBs utilize structurally benign carbonaceous materials as an anode which has a limited capacity of 372 mAh g^{-1} [1]. Diverse materials were considered as an alternative to this material such as non-carbonaceous metal alloy anodes with better capacity. Tin (Sn) metal is one of these prospective candidates which has attracted a great attention due to its low cost and high theoretical capacity of 994 mAh g^{-1} [2–4]. However, despite this advantage, a critical issue restricting its use as an anode in LIBs is found to be severe capacity degradation upon repeated insertion-extraction of Li^+ ions, which results mainly from pulverization of active material caused by a huge volume change during charge and discharge [5,6]. One way to circumvent and reduce such volume expansion is to form intermetallic compounds where one metal is inactive with respect to the alloying with Li^+ ions while Sn is active. Many successful intermetallids were reported such as Cu-Sn [7–9], Co-Sn [10–12], Ni-Sn [13–15] and Fe-Sn [16,17]. However, despite the efforts on designing such intermetallic electrodes, they still suffer from poor cyclability compared with conventional carbonaceous anodes [18] meaning that inactive component fails to mitigate the shear stress build-up at the electrode-current collector interface due to a volume expansion of the electrode, which leads to separation and isolation of the active electrode material. One of the strategic approaches to avoid such degradation could be the use of current collectors with the high surface area so the interfacial stress could be distributed evenly throughout the whole surface and alleviated along the large surface area.

A three-dimensional architecture was proposed as a step change that can provide new exciting opportunities to significantly improve the performance of LIBs. Accordingly, various concept designs of three-dimensional anodes and cathodes have been proposed and demonstrated [19–21]. Among these three-dimensional structures, foams were found to be ideal to realize a three-dimensional structure with the simultaneously high surface area, sufficient electronic conductivity to enable stable cycling, ample space to accommodate the volume changes, as well as good compatibility with the other components such as electrolyte and separator [22,23]. Thus, combining the promising Sn with transition metals and elaborately tailoring the structure of such compounds to effectively accommodate the volume expansion might allow obtaining an anode material with an outstanding performance. In this system, a thin film of active material would make it possible to increase the power density by reducing the diffusion path length of the Li^+ ions and the large surface area would make it possible to obtain high energy density. Conformal deposition by one of the cheap and simple methods as electrodeposition would allow avoiding the use of additional components like conductive additive or binders which are required based on the classical assembly procedure for LIB electrodes.

Herein we report on the three-dimensional architecture anode based on an ultrathin intermetallic alloy Ni_3Sn_4 which is carefully coated to widely available nickel (Ni) foam current collector by electrodeposition to optimize the ionic and electronic current paths to boost the power and

energy densities available per footprint area. Along with tremendous surface area, high mesoporosity, good electric conductivity, Ni foam offers an excellent chemical stability in a wide variety of liquid electrolytes.

2. EXPERIMENTAL

Anode preparation. To prepare three-dimensional negative electrodes, ultrathin active material based on Ni_3Sn_4 alloy was electrodeposited on a 1.6 mm thick commercially available mesoporous Ni foam purchased from Goodfellow, which possesses a three-dimensional structure with ≥95% porosity (80-110 pores per inch) and average hole sizes of 200-220 μm. Prior to electrodeposition, the foam was washed with ethanol then soaked into HCl/water (1:1 in volume) for 5 s to remove native oxide layers and other unwanted contaminants. After, the Ni foam was washed several times with deionized water with the consequent soaking in wetting agent sodium dodecyl sulfate (SDS). It is very vital to handle the foam with great care as it has very fragile struts (whisks) that can be easily indented. After the cleaning process, 1.6 cm discs were cut from the Ni foam to proceed with the next step.

The electrodeposition procedure took place in a two-electrode beaker cell where platinum (Pt) foil served as a counter electrode while nickel foam was used as a working electrode. The electrodeposition bath solution [24,25] consisted of 0.15 mol dm^{-1} $SnCl_2•2H_2O$, 0.1 mol dm^{-1} $NiCl_2•6H_2O$, 0.5 mol dm^{-1} $K_4P_2O_7$, and 0.125 mol dm^{-1} glycine in 2/98 vol. % ethanol/water solution with 0.1 g L^{-1} SDS. To avoid and prevent the formation of unwanted oxides or other composites the local pH at the electrode was controlled thoroughly. The pH of the bath solution was adjusted to 8 by using a diluted solution of NH_4OH. As the morphology and amount of Ni_3Sn_4 grown onto the Ni foam can be controlled by changing the potential of electrodeposition process, the procedure was conducted at different potentials of 1.0 V, 1.5 V, and 1.75V with the constant time of 10 min at a temperature of 50 ^oC using HP Hewlett-Packard 66312A potentiostat.

Characterization. X-ray diffractometer (SmartLab, Rigaku Co., Japan) was employed to identify the structure and phases of the obtained alloys. The surface morphologies of the samples were analyzed by scanning electron microscope (SEM, JSM-7500F JEOL, Japan) coupled with energy-dispersive X-ray spectroscopy (SEM-EDS, USA) to observe the homogeneity of the elemental distribution.

Electrochemical characterization. CR2032 type half-cell coin-cells were assembled in Ar-filled glove box to determine the electrochemical activity of as-prepared Ni_3Sn_4 intermetallic alloys. The electrodeposited Ni foam was sandwiched with Li metal as a reference electrode and a Celgard 2400 type microporous separator soaked in an electrolyte consisting of 1M $LiPF_6$ in a mixture of ethylene carbonate (EC)/ethyl-methyl carbonate (EMC)/dimethyl carbonate (DMC) 1:1:1 vol.%). Cyclic voltammetry was performed at the scan rate of 0.5 mV s^{-1} between 0.01 and 1.5 V at room temperature with a VMP3 potentiostat/galvanostat (Bio-Logic Science Instrument Co.). Galvanostatic charge-discharge tests were carried on a multi-channel battery testing system (BT-2000, Arbin Inc., and Neware Battery tester, Neware Co.) at the current density of 1/5 C, between 0.01 and 1.5 V at room temperature.

3. RESULTS AND DISCUSSION

The XRD patterns obtained from pristine and as-electrodeposited Ni foams are presented in Fig.1. Pristine Ni foam possesses certain distinct peaks situated at 44.5°, 51.8°, and 76.4° which coincide with the crystal planes of nickel metal, as expected [26,27]. On the as-electrodeposited sample (at 1.75 V) along with the peaks resulted from the Ni foam several peaks at 30.6°, 44.8°, 55.13° and 60.11° can be observed. According to the previous published papers, the peaks were identified to correspond to the main phase of intermetallic alloy Ni_3Sn_4 [28–30]. That leads us to the assumption that presumably, all Ni in the electrolyte bath alloyed to form Ni_3Sn_4 phase. No other impurities were detected from the XRD spectra on both pristine and electrodeposited Ni foams. It is very hard to tell if the foam itself goes through the process of alloying with Sn from the electrolyte. For this work, we speculate that the Ni foam stayed intact during the electrodeposition procedure.

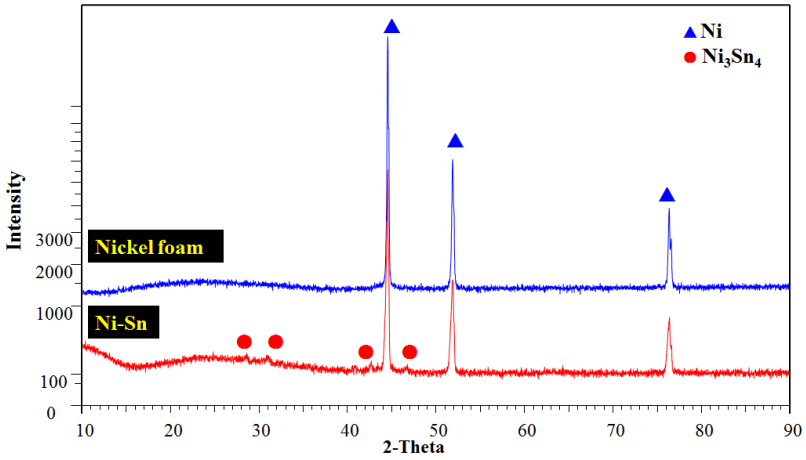

Figure 1. XRD patterns of pristine and as-electrodeposited (at 1.75 V) Ni foams

Fig. 2a-d demonstrates the surface SEM images of pristine and as-electrodeposited Ni foams. Originally pristine Ni foam has a relatively smooth surface, as seen in Fig. 2a. Coating with the alloy results in a completely rough surface with the particles agglomerated resembling cauliflower-like shapes. It can be clearly observed that the surface morphology of the alloys changes with the electrodeposition parameter - potential. The sample obtained at 1 V has well-formed and tightly packed islands formed by the primary particles with the sizes ranging between 0.5-0.7 μm (Fig. 2b). However, the morphology of the surface greatly changes for the samples electrodeposited at 1.5 V and 1.75 V (Fig. 2c, d). The cauliflower islands start to grow forming well defined half spheres with open pores. Highly porous cauliflower-like morphologies were reported to give rise to a high reversible capacity and favorable cyclability [30–32]. Observing the inset SEM images of three samples, one can be assured that the mesoporosity of the Ni foam was maintained perfectly throughout the structure after electrodeposition which will provide adequate room for the Ni_3Sn_4 alloy to expand in volume during lithiation process. Fig. 2e represents the cross-sectional view of the Ni foam strut (whisk)

coated with the alloy at 1 V. The ultrathin thickness of the as-electrodeposited alloy film can be clearly observed.

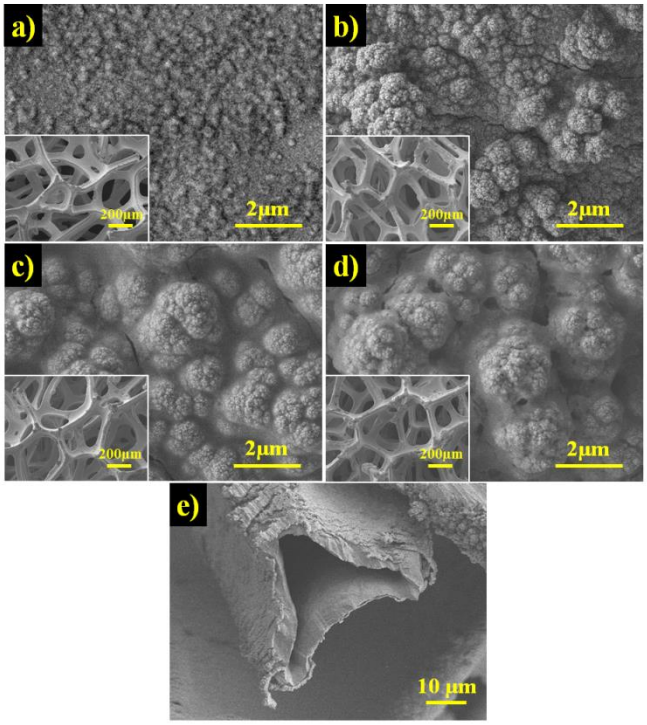

Figure 2. SEM images of pristine Ni foam (a), as-electrodeposited Ni_3Sn_4 samples prepared at (b) 1 V, (c) 1.5 V, (d) 1.75 V and (e) cross-sectional view of the as-prepared Ni_3Sn_4 sample

SEM-EDX images of three samples presented in Fig. 3 reveal elemental maps of alloy constituents Ni and Sn. All image results show a uniform distribution of elements throughout the entire framework of Ni foam confirming that the struts and interior of foam has been homogeneously and conformally coated with Ni and Sn, which assures the co-deposition of two metals onto Ni foam simultaneously. The intensity of both elements grows with the increasing potential which is in a good agreement with the assumption that with the increase in potential more active material forms. Tin's intensity in each sample amplifies with the increase in potential in comparison to Ni reassuring the existence of phase Ni_3Sn_4 which has a Ni: Sn = 43:57 atomic ratio. The quantitative analysis provided along with the elemental maps shows that the atomic ratios of Ni: Sn were 73.6:26.4, 62:38 and 58.2:41.8 for samples prepared at 1 V, 1.5 V and 1.75 V, respectively. The discrepancy in the Ni atomic ratios might be explained by the thickness of the alloy. For the sample prepared at 1V, the alloy was thin enough for the signal from the Ni foam to interfere with the signal from Ni_3Sn_4 alloy phase. However, with the increase in potential the thickness of the alloy increases as well, and the atomic ratio of Ni decrease, showing perfect fitted Ni: Sn ratio with the Ni_3Sn_4 alloy phase for the sample prepared at 1.75 V.

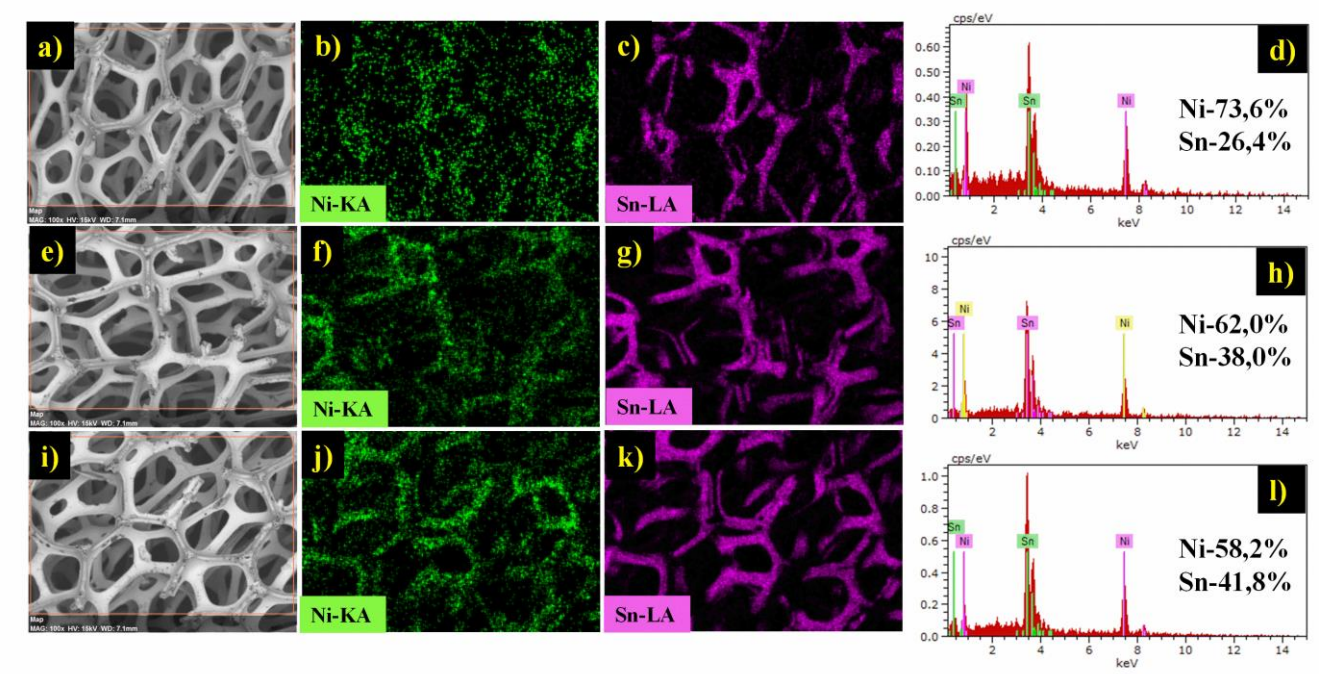

Figure 3. Representative SEM images, EDX elemental analysis and corresponding spectrum of as-electrodeposited Ni_3Sn_4 samples prepared at (a-d) 1 V, (e-h) 1.5 V and (i-l) 1.75 V

Fig. 4 illustrates the cyclic voltammetry results obtained for three Ni_3Sn_4 alloy electrodes at a scanning rate of 0.5 mV s^{-1} in the voltage window of 0-2 V. All samples possess several distinctive anodic and cathodic peaks which correspond to the alloying and dealloying of Ni_3Sn_4 with Li^+ ions reversibly during intercalation/deintercalation processes. All peaks appear at the same potentials for all three samples indicating similar electrochemical reactions. The initial charges of all samples appear to be different from consequent charges. This can be explained by the activation of the alloy along with some changes in the electrodes states that modifies the electrodes to a stable structure where the succeeding reactions repeat reversibly [15]. Each anodic peak represents the electrochemical reaction between different phases of alloy with Li^+ ions which correlates with the multistep lithiation [33]. It appears that the initial lithiation process for our as-electrodeposited alloy is very unique. Judging the three samples' cathodic peaks one can observe that they all appear at the same potentials over all the cycles without significant changes. It should be noted that the magnitude of the peaks amplifies with the increasing electrodeposition potential.

The charge-discharge profiles of three Ni_3Sn_4 alloy electrodes obtained at 1/5 C rate in the voltage window of 0.01-1.5 V are illustrated in the Fig. 5. All three samples' charge-discharge curves exhibit several voltage plateaus indicating a stepwise insertion/deinsertion of Li^+ ions into/from the active material structure [34,35]. During the first charge, the potentials of all three samples drop rapidly from OCV (open circuit voltage) to about 0.3 V, stabilize and then gradually decrease delivering charge capacities of 650 mAh g^{-1}, 500 mAh g^{-1} and 700 mAh g^{-1}, respectively. Theoretically, the specific capacity of the Ni_3Sn_4 alloy is reported to be 725 mAh g^{-1} [36], but smaller than this value were previously reported [24,37,38], and assumed to be caused by a limited

consumption of the active material by the alloying reaction [39]. The long plateaus at approximately 0.3 V possessed by all samples suggest that the Sn atoms segregate from the Ni_3Sn_4 alloy phase and alloys with the Li^+ ions resulting in a Li_xSn phase.

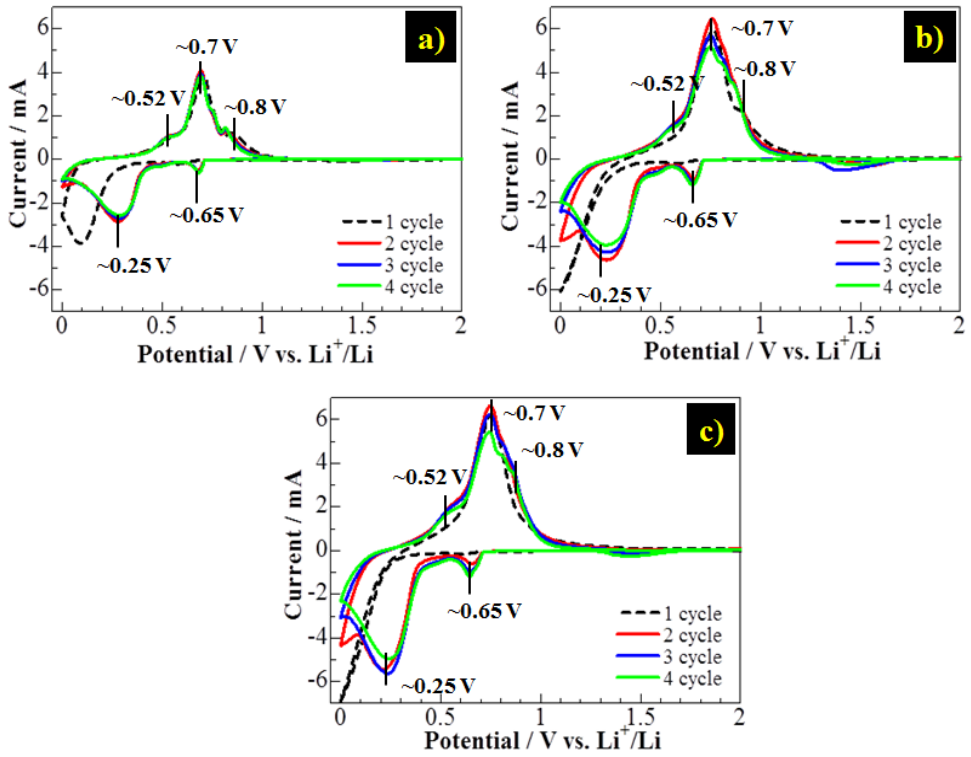

Figure 4. Cyclic voltammograms of as-electrodeposited Ni_3Sn_4 samples prepared at (a) 1 V, (b) 1.5 V and (c) 1.75 V at the scanning rate 0.5 mV s^{-1} in the voltage range of 0-2 V

A gradual decrease of the potential after plateaus results from the coexistence of several Li_xSn_y alloy phases such as Li_7Sn_3, Li_5Sn_2, $Li_{13}Sn_5$, Li_7Sn_2 and $Li_{22}Sn_5$ in active material [33]. With discharge, Li^+ ions are deintercalated from different Li_xSn_y phases, and freed Sn atoms get absorbed into the Ni matrix anew to form the initial Ni_3Sn_4 alloy. The initial discharge capacities delivered were 500, 420, and 580 mAh g^{-1} for the samples electrodeposited at 1V, 1.5 V, and 1.75 V, respectively, with the little capacity loss which is attributed to the SEI formation [39]. Starting from the second charge new plateau appears at approximately 0.65 V which is responsible for alloying of free Sn with the Li^+ ions in all samples with the implication that not all Sn atoms get absorbed into the matrix [29]. With the further cycling, the plateaus indicating the reaction of Sn with Li^+ ions get more pronounced meaning that more Sn atoms stay free. Similar voltage profiles of the Ni-Sn alloys coated on the Cu foam [28] and Cu foil [40] were reported with the reversible capacities of 440 mAh g^{-1} and 388.9 mAh g^{-1}, respectively, which are slightly lower than three-dimensional Ni_3Sn_4 electrodes obtained in this work. We speculate that the free Sn atoms get trapped inside the Ni matrix where the volume expansion is suppressed by the matrix structure.

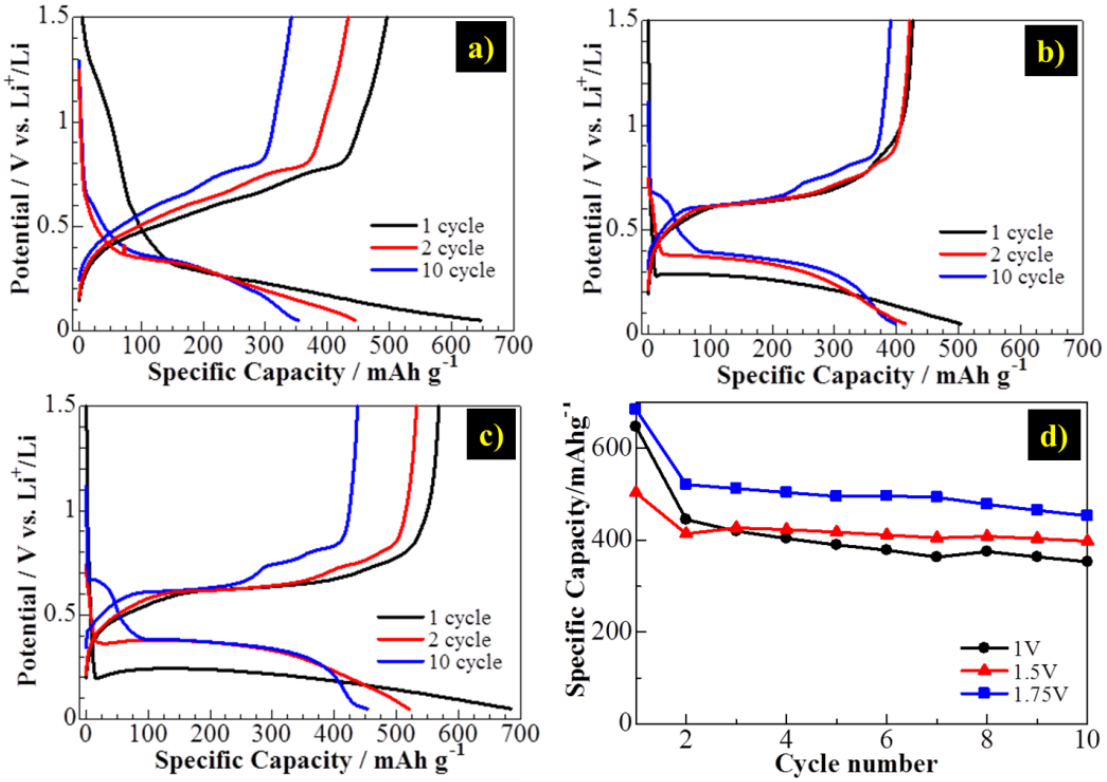

Figure 5. Charge-discharge profiles of Ni_3Sn_4 samples prepared at (a) 1 V, (2) 1.5 V and (3) 1.75 (V), and cyclability of Ni_3Sn_4 samples at 1/5 C rate and voltage window 0.01-2 V

Fig. 5d shows the cycling behavior of three samples cycled at 1/5C rate between 0.01 and 1.5 V for 10 cycles. Capacity retention of all three samples is stable and satisfactory without any abrupt changes in capacity. After 10^{th} cycle samples exhibited 350 mAh g^{-1}, 400 mAh g^{-1} and 451 mAh g^{-1} for anodes prepared at 1 V, 1.5 V and 1.75 V, respectively. The better capacity retention of all samples can be explained by the combined effect of Ni matrix and enhanced ability of the 3D structured Ni foam to buffer the stress induced during the lithiation and delithiation processes. Although the sample obtained at 1.75 V showed a good specific discharge capacity, its performance (cyclability and stability) is not yet fully satisfactory.

4. CONCLUSION

To conclude, the three-dimensional anode was prepared by means of utilizing commercially available three-dimensional Ni foam with the Ni_3Sn_4 alloy electrodeposition directly on its surface. The as-electrodeposited anodes exhibited satisfactory capacity and stable capacity retention over 10 cycles. The best electrodeposition condition was found to be relatively high voltage (1.75 V) for a limited time of 10 min which resulted in an uneven deposition with highly porous cauliflower-like morphology. The large surface area of the foam allowed incorporating a reasonable amount of active material per footprint area. The foam itself acted as a current collector providing fast diffusion paths for Li^+ ions. The direct contact between ultrathin alloy and the current collector, sufficient space

available due to the mesoporosity, as well as high surface area accounts for the satisfactory performance of the as-prepared three-dimensional structured anode. Thereupon, the as-prepared 3D structured anode exhibited good Li^+ ions storage performance when they were directly employed as LIB anodes. The efficiency of the Ni as the matrix was indicated from the galvanostatic cycling test where adequate cyclability was confirmed. Further optimization of the electrodes by changing the electrodeposition conditions for enhancing the capacity and stability is underway.

ACKNOWLEDGMENTS
The work has been supported by the research grant AP05133706 “Innovative high-capacity anodes based on lithium titanate for a next generation of batteries” and targeted program No. 0115PK03029 “NU-Berkeley strategic initiative in warm-dense matter, advanced materials, and energy sources for 2014-2018” from the Ministry of Education and Science of the Republic of Kazakhstan.

CONFLICT OF INTEREST
The authors declare that they have no conflict of interest.

References

1. J.L. Tirado, *Mater. Sci. Eng. R Reports*. 40 (2003) 103.
2. H. Tian, F. Xin, X. Wang, W. He, W. Han, *J. Mater.* 1 (2015) 153.
3. R.Z. Hu, H. Liu, M.Q. Zeng, J.W. Liu, M. Zhu, *Chinese Sci. Bull*. 57 (2012) 4119.
4. L. Liu, F. Xie, J. Lyu, T. Zhao, T. Li, B.G. Choi, *J. Power Sources*. 321 (2016) 11.
5. B. Wang, B. Luo, X. Li, L. Zhi, *Mater. Today*. 15 (2012) 544.
6. J.J. Wang, Y.C.K. Chen-Wiegart, J.J. Wang, *Angew. Chemie - Int. Ed.* 53 (2014) 4460.
7. N. Tamura, R. Ohshita, M. Fujimoto, S. Fujitani, M. Kamino, I. Yonezu, *J. Power Sources*. 107 (2002) 48.
8. K.D. Kepler, *Electrochem. Solid-State Lett*. 2 (1999) 307.
9. D.B. Polat, J. Lu, A. Abouimrane, O. Keles, K. Amine, *ACS Appl. Mater. Interfaces*. 6 (2014) 10877.
10. F.S. Ke, L. Huang, H.B. Wei, J.S. Cai, X.Y. Fan, F.Z. Yang, S.G. Sun, *J. Power Sources*. 170 (2007) 450.
11. D. Larcher, L.Y. Beaulieu, O. Mao, A.E. George, J.R. Dahn, *J. Electrochem. Soc*. 147 (2000) 1703.
12. J. Zhang, Y. Xia, *J. Electrochem. Soc*. 153 (2006) A1466.
13. R. Hu, H. Liu, M. Zeng, J. Liu, M. Zhu, *J. Power Sources*. 244 (2013) 456.
14. H. Mukaibo, T. Momma, M. Mohamedi, T. Osaka, *J. Electrochem. Soc*. 152 (2005) A560.
15. J. Hassoun, S. Panero, B. Scrosati, *J. Power Sources*. 160 (2006) 1336.
16. O. Mao, *J. Electrochem. Soc*. 146 (1999) 405.
17. C.J. Liu, F.H. Xue, H. Huang, X.H. Yu, C.J. Xie, M.S. Shi, G.Z. Cao, Y.G. Jung, X.L. Dong, *Electrochim. Acta*. 129 (2014) 93.
18. F. Yao, D.T. Pham, Y.H. Lee, *ChemSusChem*. 8 (2015) 2284.
19. J.W. Long, B. Dunn, D.R. Rolison, H.S. White, *Chem. Rev*. 104 (2004) 4463.
20. T.S. Arthur, D.J. Bates, N. Cirigliano, D.C. Johnson, P. Malati, J.M. Mosby, E. Perre, M.T. Rawls, A.L. Prieto, B. Dunn, *MRS Bull*. 36 (2011) 523.
21. M. Roberts, P. Johns, J. Owen, D. Brandell, K. Edstrom, G. El Enany, C. Guery, D. Golodnitsky, M. Lacey, C. Lecoeur, H. Mazor, E. Peled, E. Perre, M.M. Shaijumon, P. Simon, P.-L. Taberna, *J. Mater. Chem.* 21 (2011) 9876.

22. A. Mukanova, A. Nurpeissova, A. Urazbayev, S.S. Kim, M. Myronov, Z. Bakenov, *Electrochim. Acta*. 258 (2017) 800.
23. J. Yuan, C. Chen, Y. Hao, X. Zhang, R. Agrawal, W. Zhao, C. Wang, H. Yu, X. Zhu, Y. Yu, Z. Xiong, Y. Xie, *J. Alloys Compd*. 696 (2017) 1174.
24. H. Mukaibo, T. Sumi, T. Yokoshima, T. Momma, T. Osaka, *Electrochem. Solid-State Lett.* 6 (2003) A218.
25. B. Tolegen, A. Adi, A. Aishova, Z. Bakenov, A. Nurpeissova, *Mater. Today Proc.* 4 (2017) 4491.
26. K. Zhuo, M.G. Jeong, C.H. Chung, *J. Power Sources.* 244 (2013) 601.
27. S. Sengupta, A. Patra, A. Mitra, S. Jena, K. Das, S.B. Majumder, S. Das, *Appl. Surf. Sci*. 441 (2018) 965.
28. L. Huang, H.-B. Wei, F.-S. Ke, X.-Y. Fan, J.-T. Li, S.-G. Sun, *Electrochim. Acta*. 54 (2009) 2693.
29. H. Mukaibo, T. Momma, T. Osaka, *J. Power Sources*. 146 (2005) 457.
30. J. Hassoun, S. Panero, B. Scrosati, *J. Power Sources*. 160 (2006) 1336.
31. D. Zhang, C. Yang, J. Dai, J. Wen, L. Wang, C. Chen, *Trans. Nonferrous Met. Soc. China* (English Ed. 19 (2009) 1489.
32. O. Crosnier, T. Brousse, X. Devaux, P. Fragnaud, D.M. Schleich, J. Power Sources. 94 (2001) 169.
33. D. Jiang, X. Ma, Y. Fu, *J. Appl. Electrochem*. 42 (2012) 555.
34. M. Winter, J.O. Besenhard, *Electrochim. Acta.* 45 (1999) 31.
35. J. Hassoun, S. Panero, P. Reale, B. Scrosati, *Int. J. Electrochem. Sci*. 1 (2006) 110.
36. H. Tian, F. Xin, X. Wang, W. He, W. Han, *J. Mater*. 1 (2015) 153.
37. J. Hassoun, S. Panero, B. Scrosati, *J. Power Sources*. 160 (2006) 1336.
38. K. Nishikawa, K. Dokko, K. Kinoshita, S.-W. Woo, K. Kanamura, *J. Power Sources.* 189 (2009) 726.
39. J.-T. Li, J. Światowska, V. Maurice, A. Seyeux, L. Huang, S.-G. Sun, P. Marcus, *J. Phys. Chem*. C. 115 (2011) 7012.
40. W. Deng, X. Wang, C. Liu, C. Li, M. Xue, R. Li, F. Pan, *ACS Appl. Energy Mater*. 1 (2018) 312